Grafting carbon dots on persistent luminescence phosphors to generate remarkably improved NIR afterglow for microenvironment fluorescence detection

Junqing Xiahou, Li Cao, Sai Huang, Tao Zhang, Ji-Guang Li, and Qi Zhu**

J. Xiahou, L. Cao, Q. Zhu

Key Laboratory for Anisotropy and Texture of Materials (Ministry of Education),

School of Materials Science and Engineering,

Northeastern University,

Shenyang, Liaoning 110819, PR China

Tel: +86-24-8367-2700

E-mail: zhuq@smm.neu.edu.cn

S. Huang

School of Material Science and Engineering,

University of Jinan,

Jinan, China

T. Zhang, Q. Zhu

Shenyang National Laboratory for Materials Science,

Northeastern University,

Shenyang, Liaoning 110819, PR China

J.-G. Li

Research Center for Electronic and Optical Materials,

National Institute for Materials Science,

Tsukuba, Ibaraki 305-0044, Japan

Tel: +81-29-860-4394

E-mail: LI.Jiguang@nims.go.jp

Keywords: CDs coating; energy transfer; composite luminescent materials; acid microenvironment detection

Abstract

Recently, combining long afterglow materials with organic fluorescent dyes, particularly carbon dots (CDs) to produce heterojunction and improve its luminescence and persistence properties became an important research direction. However, the precise role of these internal defects in the energy transfer process of CD@inorganic matrix composite fluorescent materials has not been thoroughly discussed. Establishing matching trap level to promote the energy transfer between the trap level and CDs level not only helps to enhance the afterglow performance, but also can explain the heterogeneous structure interaction between organic-inorganic fluorescent materials. Herein, ZLAGC@CDs luminescent composite was successfully synthesized via coating CDs on $Zn_{1-x}(Li/Al)_xGa_{2x}O_4$:0.005$Cr^{3+}$ (ZLAGC, x=0-1), which exhibits a unique double emission at ~430 nm (the defect luminescence of CDs) and 718 nm (the $^2E \rightarrow {}^4A_2$ transition of Cr^{3+}). After coating, the energy transfer from the defect level of CDs to the excited state of Cr^{3+} enhanced the NIR emission. The electron transfer between the defect level of CDs and the split deeper trap level of ZLAGC also improved the visible and near-infrared (NIR) afterglow. The fluorescence and afterglow signals of ZLAGC@CDs are highly sensitive to solution pH under acidic conditions, indicating that the prepared fluorescent composite has potential application in acid microenvironment fluorescence detection.

1. Introduction

In recent years, Cr^{3+}-doped zinc gallate near-infrared (NIR) persistent luminescence phosphors (PLPs) have become a hotspot in the research field of persistent luminescence and bioimaging because of the NIR emission and long afterglow properties[1]. The NIR PLPs based on $ZnGa_2O_4$:Cr^{3+} (ZGC) can be excited by various light sources, and their traps can store and release light energy after excitation, resulting in a unique time separation between excitation and emission, which could prevent self-fluorescence interference from the excitation light and make them become potential fluorescence sensing as well as detection materials[2]. Although much progress has been made in the study of ZGC, there is still ample room for further improvement in the application of NIR persistent luminescence signals in these nano particles, beyond regulating their crystal structure and inherent traps[3]. This limitation arises from the fact that the emission of the NIR PLPs is solely due to the absorption and emission of the doped Cr^{3+} ions in the ZGC. However, the concentration of Cr^{3+} ions must be kept extremely low in NIR PLPs (only a molar concentration of 0.5%), which limits light absorption in ZGC[4]. Therefore, designing and preparing new long persistent luminescence materials with excellent performance and practicality by combining long afterglow luminescence with special frequency band luminescence became an important research direction[5].

Organic fluorescent dyes, particularly carbon dots (CDs), possess strong absorption and high emission efficiency[6]. These properties have been utilized to enhance the luminescence of inorganic phosphors through sensitization. CDs have small sizes, high specific surface areas, and rich surface functional groups, making them easily interact with chemical substances or be influenced by environmental factors, resulting in changes in optical properties, which makes CDs be developed into various sensors[7]. Sensitizing inorganic phosphors by combining organic dyes has been extensively discussed. For instance, utilizing the overlap of emission of CDs and absorption of activation ions, such as Yb, Nd, and Cr ions can effectively sensitize inorganic phosphors and enhance their quantum efficiency[8]. Another study by Yu and

colleagues focused on improving the stability and red luminous efficiency of Mn^{2+} doped CDs@Zeolite Composites by energy transfer[9]. And the sensitization strategy employed by using the organic Rhodamine dye (5-carboxy-tetramethylrhodamine, TAMRA) also improved the luminescence and persistent luminescence signal of ZGC PLPs[10]. Furthermore, the mechanism of energy transfer in CD@inorganic matrix composite fluorescent materials has not been thoroughly investigated. CDs are known to be embedded in various materials, resulting in the formation of CDs-based afterglow materials, which is achieved through structural constraints and chemical bonds between the rigid matrix and the internal CDs, such as coordination bonds, covalent bonds, and hydrogen bonds. The integration of CDs fluorescent dyes with inorganic materials requires an effective driving force to the co-assembly of the CDs and the inorganic material. It is a promising method to sensitize PLPs by using CDs and long-persistence materials to produce heterojunction and improve its luminescence and persistence properties. Lu et al. have made significant progress in enhancing weak phosphorescent light and utilizing defection-stabilized triplet excitons to produce ultra-long and efficient CDs afterglow materials under visible light[11]. In another study, Hu et al. implemented core-satellite structures with amorphous silica decorated with CDS. Traps in these structures can capture and release electrons, which provide a stable triplet exciton[12]. Additionally, CDs@$ZnAl_2O_4$ composites were prepared by a simple calcination method, where CDs were embedded in the stable matrix structures[13]. The multi-emission afterglow properties of the CDS were primarily derived from various triplets produced by the matrix-assisted system and the trap-stabilized triplet excitons under different crossing paths between the systems. It is important to understand how the internal defects of inorganic substrates contribute to the energy transfer process. However, the precise role of these internal defects in the energy transfer process of CD@inorganic matrix composite fluorescent materials has not been thoroughly discussed.

On the one hand, the $Zn_{1-x}(Li/Ga)_xGa_2O_4$:0.005Cr^{3+} phosphors developed in our previous study, possesses both deep and shallow traps[2d]. The deep traps allow for direct transfer of electrons to similar energy levels through tunneling, which

contributes to the persistence of luminescence. On the other hand, increasing the calcination temperature enhances the absorption of visible light by Cr^{3+} ions[14]. Additionally, CDs exhibit numerous energy levels concentrated in the visible region, which is related to the defects. By combining CDs (construction external defects) with NIR PLPs, the matching of energy levels for PLPs and external defect CDs can be achieved, thereby enhancing the energy transfer between traps and external defects. In this study, spinel-structured phosphors $Zn_{1-x}(Li/Al)_xGa_2O_4:0.005Cr^{3+}$ (x=0-1) were synthesized solid phase method. The strategy of energy transfer between CDs and Cr^{3+} ions was employed to enhance the NIR persistent luminescence. The hydrothermal method was used to combine CDs with $Zn_{1-x}(Li/Al)_xGa_2O_4:0.005Cr^{3+}$ to create ZLAGC@CDs composite luminescent materials. The occupancy of [Li^+-Al^{3+}] substituents in the lattice was analyzed, and their effects on trap depth and luminescence properties were investigated. Furthermore, the luminescence mechanism and energy transfer mechanism of the ZLAGC@CDs composites were revealed. By studying the relationship between pH change and luminescence intensity, the relationship between pH change and optical properties was uncovered. Additionally, the potential application of ZLAGC@CDs composites in fluorescence detection of microenvironment changes was explored.

2. Experimental section

2.1 Synthesis of inorganic fluorescent powders

Inorganic fluorescent powders containing special chemical compositions of $Zn_{1-x}(Li/Al)_xGa_2O_4:0.005Cr^{3+}$ (x=0-1) were synthesized using ZnO, Al_2O_3, Ga_2O_3, Cr_2O_3, and Li_2CO_3 with a purity of 99.99% as raw materials (Aladdin Chemical Reagent Co., Ltd., Shanghai, China). Firstly, all the raw materials were mixed by a mortar and pestle for 30 min to ensure thorough mixing, according to the stoichiometric ratio of $Zn_{1-x}(Li/Al)_xGa_2O_4:0.005Cr^{3+}$. The mixture was then preheated at 900°C in an alumina crucible under an oxygen atmosphere for 4 h. Then the sample was cooled to room temperature and ground for an additional 30 min and then heated at 1400°C under an oxygen atmosphere for 4 h to obtain the final inorganic phosphors.

The heating rate for both heating steps was set at 5°C/min.

2.2 Synthesis of CDs and composite fluorescent materials

CDs and ZLAGC@CDs composite fluorescent powders were prepared using a hydrothermal method. The experimental materials (citric acid, urea, DMF, ZLAGC) were added to a beaker in different proportions and stirred magnetically for 30 min. Then the mixture was transferred to a 100 mL hydrothermal reactor and reacted at a fixed temperature (90, 120, 140, 160 °C) in a preheated oven for a certain period of time (2, 4, 6 h). After the reactor was cooled, the products were collected by centrifugation at high speed, washed with water and ethanol, then dried at in an oven to obtain the samples.

2.3 Characterization techniques

To identify the phase, X-ray diffraction (XRD, Model SmartLab, Rigaku, Tokyo, Japan) was used with Cu Kα radiation filtered through nickel, and the scan rate is 10°2θ/min. With the assistance of the field emission scanning electron microscopy (FE-SEM, Model JSM-7001F, JEOL, Tokyo) and transmission electron microscopy (TEM, Model JEM-2000FX, JEOL, Tokyo), the he morphology of the products was observed. X-ray photoelectron spectroscopy (XPS) measurements were performed using the Model Axis Supra instrument (Kratos Analytical Ltd., Manchester, UK). The measurements were conducted in an ultra-high vacuum chamber with monochromatic Al Kα X-ray radiation, and the pressure is below 3×10^{-9} Torr. Then the binding energy was calibrated with the C1s peak at 284.8 eV. Fourier transform infrared spectroscopy (FT-IR) was conducted by Nicolet iS5 (Thermo Fisher Scientific, USA) with the KBr as standard. Fluorescence properties of the fluorescent powders were analyzed using a fluorescence spectrophotometer (FP-8600, Jasco Corporation, Tokyo, Japan) and a JY FL3-21 spectrophotometer (Horiba, Kyoto, Japan). Excitation was performed with the xenon lamp (450 W), the slits were set at 10 nm for FP-8600 and 2 nm for JY FL3-21. The JY FL3-21 spectrophotometer was used to analyze the persistent luminescence with slits set at 20 nm for both excitation and emission. Prior to thermoluminescence (TL) measurement, the sample was exposed under the 254 nm UV light (15 W) and ~740 nm NIR LED light (25 W), and

TL emission curves were recorded using FJ427A1 TL dosimeter (Beijing Nuclear Instrument Factory) at a heating rate of 1 K/s. NIR afterglow was captured using a P4-0118 night vision device.

3. Results and discussion

3.1 Synthesis of persistent luminescent phosphor with splitted electron traps

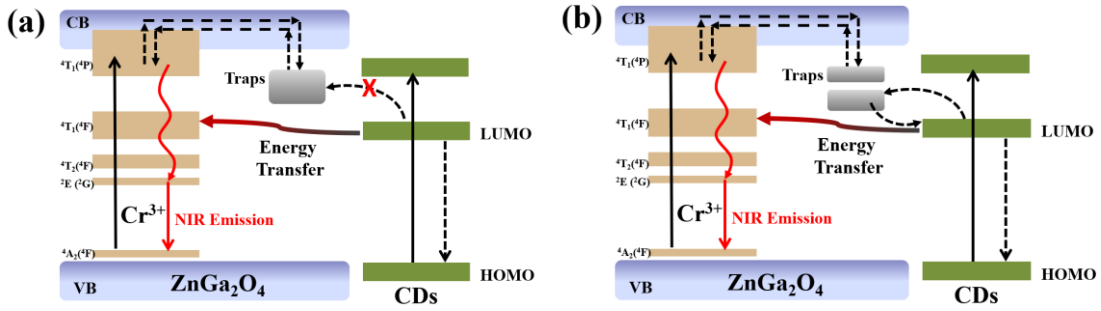

Figure 1. A model of an energy level diagram depicting the energy transfer process between phosphors and CDs. (a) Traditional energy transfer process between phosphors and CDs without carriers transition processes from CDs to shallow traps (STs). (b) Energy transfer process between phosphors and CDs with carriers transition processes from CDs to deep traps (DTs).

In theory, to enhance the luminescence and afterglow properties of NIR PLPs using Organic fluorescent dyes (CDs), it is necessary not only to find a specific frequency band for sensitive light emission to improve its emission efficiency but also to create an appropriate trap depth to facilitate tunneling in order to increase the afterglow intensity[2d, 15]. Spinel-structured $ZnGa_2O_4$:Cr^{3+} commonly exhibits a shallow trap depth, which results in a significant distance between the lowest unoccupied molecular orbital (LUMO) of CDs and the trap level, making energy transfer or tunneling effect virtually impossible (Figure 1a)[3c, 4b, 16]. Through material analysis, this study introduces the concept of the trap split NIR PLPs to capture and release carriers from LUMO, which can promote the energy transfer between the trap level and the excited state level of CDs, thereby enhancing the emission performance and long persistent luminescence signal of NIR materials (Figure 1b).

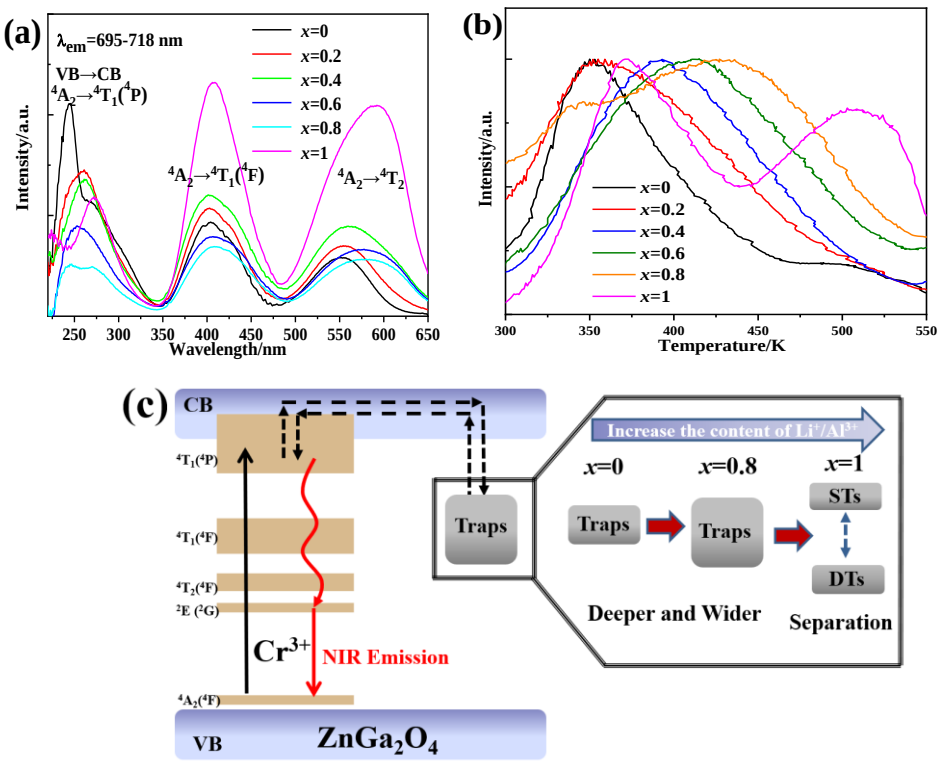

Figure 2. (a) PLE, (b) TL curves of ZLAGC samples. (c) Schematics illustrating the multi-trap energy level diagram with the increased *x* value.

To obtain inorganic phosphors with appropriate trap depth, a series of NIR PLPs $Zn_{1-x}(Li/Al)_xGa_2O_4$:0.005Cr^{3+} (ZLAGC, *x*=0-1) were designed and synthesized using a straightforward solid-phase reaction. As shown in Figure S1, the space group of spinel structure gradually changes from $Fd\bar{3}m$ (*x*<0.8, $ZnGa_2O_4$, JCPDS NO.38-1240) to $P4_332$ (*x*=1, $LiGa_5O_8$, JCPDS File No. 38-1371) with the increase of Li^+/Al^{3+} content, which also lead a reduced lattice constant (*a*=*b*=*c*) (Table S1)[2d]. As the increase of *x* value, the excitation peaks of Cr^{3+} ions shift towards longer wavelengths was demonstrated in the photoluminescence excitation (PLE) spectra (Figure 2a), which is caused by the reduced crystal field strength with the increase of Li^+/Al^{3+} doping amount (Equations S1-S5, Table S2)[17]. The photoluminescence (PL) spectra and persistent luminescence decay curves of the sample are shown in the Figure S2 and Figure S3. Previous studies have reported that crystal field changes may affect trap distribution such as the observed centroid migration in Ce^{3+} ion luminescence[2d]. Thermoluminescence (TL) curves of the ZLGGC samples were measured to investigate the trap depth and distribution, as illustrated in Figure 2b and Figure S4.

The trap depth (E) and density (n)was estimated using equations as followed[14, 18]:

$$E = T_m/500 \quad (1)$$

$$n = \omega I_m/\{\beta\times[2.52+10.2\times(\mu_g-0.42)]\} \quad (2)$$

the calculation results are presented in Table S3. As shown in Figure 2b, the TL peak gradually shifts towards higher temperatures, and the full width at half maximum (FWHM) gradually increases with an increase in the Li^+/Al^{3+} content in ZLAGC, which cause the appearance of two traps: deep traps (DTs) and shallow traps (STs). This behavior is consistent with previous studies, the increase of Li^+/Al^{3+} content leads the crystal field strength weak, resulting in deeper trap depths and wider trap energy levels (Figure 2c)[2d, 14]. The deep trap induced by this splitting creates conditions for subsequent energy transfer with CDs. To study the effect of the temperature on the ZLAGC structural, electronic and defect properties, low-temperature luminescence and thermo-luminescence measurement (Figure S5 and S6) were conducted. The NIR emissions bands are regarded as excitonic emissions rather than associated with intrinsic defects, which proves that there are no intrinsic defects in the crystal[19]. In order to further analyze the thermo-luminescence of ZLAGC, the activation energies E_a of the thermal quenching was determined by using the expression as followed[19-20]:

$$I=I_0/(1+c\exp(-E_a/k_BT)) \quad (3)$$

where I is the luminescence intensity, I_0 is the luminescence intensity at 273 K, c is a constant parameter, k_B is the Boltzmann's constant, and T is temperature. Several research discussed the temperature dependence of the emission bands in $ZnGa_2O_4:Cr^{3+}$ and $LiGa_5O_8:Cr^{3+}$, as well as gave the activation energies E_a of the thermal quenching around 0.2 eV[21]. The calculated activation energies E_a of the thermal quenching is about 0.19 eV, which is similar to the data reported in the literature.

3.2 Synthesis, structure and optical properties of ZLAGC@CDs

Based on the literature reports, luminous carbon dots (CDs) were prepared by hydrothermal synthesis using citric acid and urea as reactants (at a reactant mass ratio of 1:2), dissolved in DMF, and mixed evenly. The hydrothermal reaction was

conducted at 160°C for 4 h according to the raw material ratio specified by Li and colleagues[22]. The resulting sample was digitally photographed under an ultraviolet lamp, and it emitted yellow-green or green light under the excitation of 254 and 302 nm. Under the excitation of 365 nm, a blue-green light was emitted.

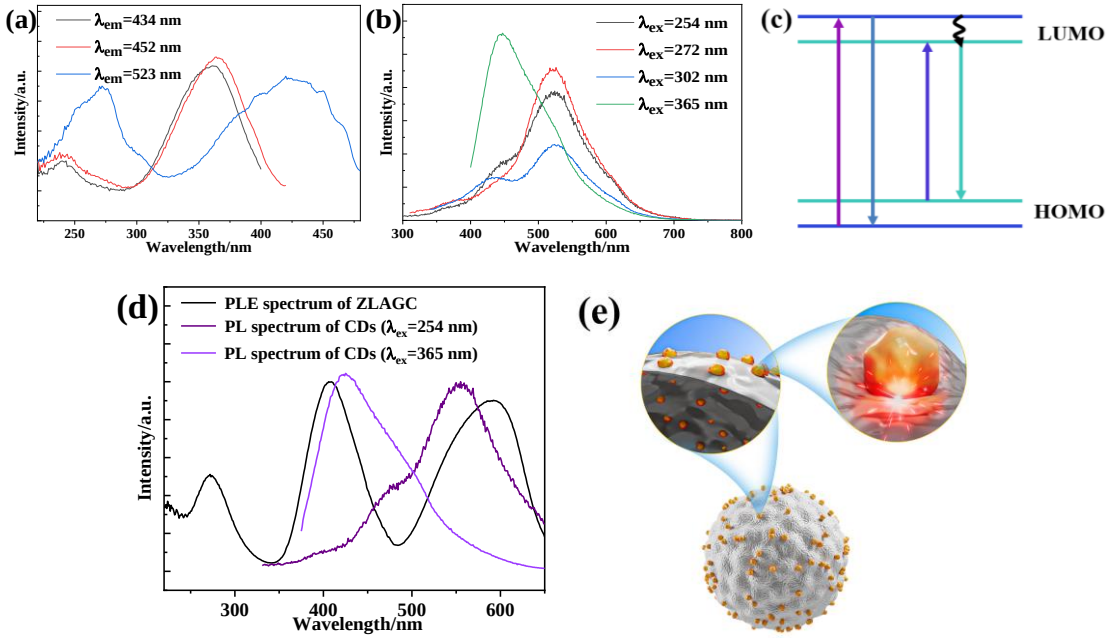

Figure 3. (a) PLE, (b) PL spectra and (c) schematic diagram of the proposed luminescence mechanism of CDs. (d) PLE spectrum of ZLAGC monitored at 718 nm and PL spectra of CDs. (e) Schematic illustration of heterojunction formation for the ZLAGC@CDs samples.

In general, CDs exhibit typical absorption in the ultraviolet region, with the main optical absorption peaks located in the ranges of 230-300 nm and 320-420 nm, corresponding to the π-π* and N-π* transition of the C=C and C=O/C=N bond, respectively[6b, 7b, 23]. The photoluminescence properties of the CDs solution were studied comprehensively. Figure 3a, 3b and S7 show the PLE/PL and UV-Vis absorption spectra of CDs in aqueous solution. Apparently, CDs water dispersion exhibited two major absorption peaks at about ~260 and ~400 nm consistent with the excitation spectrum, which proved the existence of π-π* and N-π* transitions in the CDs. Under the excitation of 254 nm, 272 nm, and 302 nm, the main peak of the PL spectrum was around 530 nm. Under the excitation of light at 365 nm wavelength, the emission peak of the PL spectrum was around 450 nm. Based on the study of the

luminescent properties of CDs, a model for the multicolor luminescence mechanism was proposed, in which the transition of electrons from the highest occupied molecular orbital (HOMO) to the lowest unoccupied molecular orbital (LUMO) can occur in different luminous centers. Through the independent absorption of photons with different energies, the excited electrons can return to the ground state by radiative transition, resulting in multicolor fluorescence emission (Figure 3c and 3d)[6b, 7a]. The ZLAGC phosphor (x=1), prepared previously, can be excited by light at ~410 nm and ~580 nm wavelengths, exhibiting a high luminescence agreement with the CDs prepared in this section (Figure 3d). Therefore, the CDs prepared by this method can be coated with ZLAGC to prepare ZLAGC@CDs composite luminescent materials, which enable energy transfer between the CDs and Cr^{3+} and promote the storage of electrons in the splitting trap to enhance afterglow luminescence (Figure 3e).

Based on the above experimental results, the hydrothermal reaction conditions were further optimized by adjusting the reaction temperature and time to prepare composite phosphors (Table S4). The digital photos of ZLAGC suspension and ZLAGC@CDs aqueous solution (0.1g/mL) prepared under different synthesis conditions were shown in Figure S8, which were under different wavelengths ultraviolet excitation. From left to right, the samples are ZLAGC, ZLAGC@CDs-1, ZLAGC@CDs-2, ZLAGC@CDs-3, and ZLAGC@CDs-4. It can be observed from the figure that ZLAGC@CDs-2 and ZLAGC@CDs-3 composite phosphor solutions emitted red light under the excitation of 254 nm and 302 nm, and blue light under the excitation of 365 nm. Among them, ZLAGC@CDs-3 (obtained after a reaction at 120°C for 6 h) exhibited the strongest luminous intensity. The aqueous solutions of ZLAGC@CDs-4 and ZLAGC@CDs-5 composite phosphors only emitted CDs light under the excitation of different ultraviolet wavelengths, without showing the NIR emission of ZLAGC. This phenomenon can be attributed to the higher reaction temperature promoting the carbonization of reactants like citric acid, and the addition of inorganic phosphor promoting heterogeneous nucleation, resulting in a thick CDs coating that shields the luminescence of ZLAGC phosphor[6a, 23]. Therefore, subsequent

experiments were conducted using the preparation conditions of the ZLAGC@CDs-6 sample.

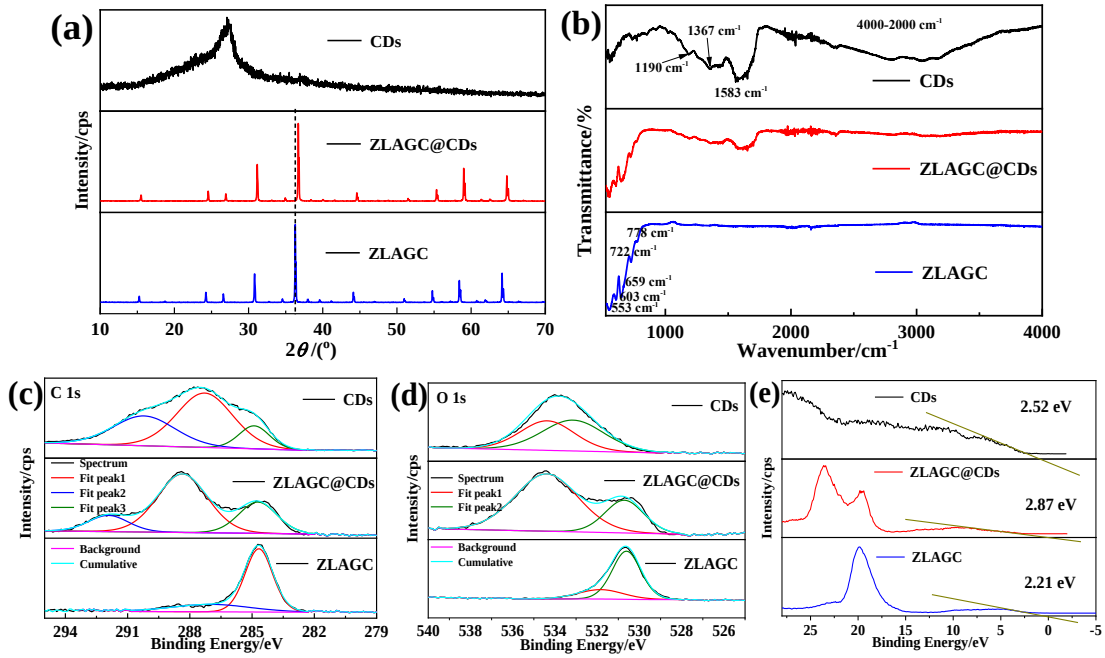

Figure 4. (a) XRD patterns, (b) FT-IR spectra, (c, d) high-resolution XPS spectra of C 1s, O 1s, and (e) Valence-band XPS spectra for CDs, ZLAGC, and ZLAGC@CDs.

To analyze the structural characteristics of composite fluorescent materials, XRD, FT-IR, XPS, SEM, and TEM analyses were performed on the prepared CDs, ZLAGC, and ZLAGC@CDs. As shown in Figure 4a, the XRD patterns of CDs woned a broad peak around 25°, indicating that CDs had an almost amorphous carbon structure. Due to the poor crystallinity of nanomaterials compared to bulk materials, CDs had many lattice defects caused by abundant surface groups, resulting in a broad peak. Compared to the XRD patterns of ZLAGC, the diffraction peak of ZLAGC@CDs shifted to higher angles, indicating a decrease in regularity after surface functionalization of CDs[11, 13]. To further confirm these results, FT-IR measurements was performed on the prepared composite materials (Figure 4b). It can be seen in the FT-IR spectrum of CDs, wide and distinct absorption peaks can be seen at 4000-2000 cm^{-1}, indicating the presence of O-H and C-H groups. The peaks associated with C-H, O-H, and N-H stretching appeared at 1583, and 1367, 1190 cm^{-1}, further indicating the presence of CDs. However, there are only 5 peaks in the FT-IR spectrum of ZLGGC[24]. The two peaks centered at 778 and 603 cm^{-1} were related to the tensile

vibration of Ga-O, the 722 cm^{-1} peaks correspond to the tensile vibration of Li-O, and the peaks centered at 553 and 659 cm^{-1} were relevant to the symmetric tensile vibration and bending vibration of Al-O, respectively. After coating, the vibration peaks of various functional groups and metal-oxygen bonds appear, which indicating CDs were coated onto the surface of ZLAGC particles[2c, 13, 25]. XPS characterizations further support this result. Figures 4c, Table S5 and Figures 4d, Table S6 showed the high-resolution C 1s and O 1s spectra of the prepared samples, respectively. After CD encapsulation, the peaks of O 1s, C 1s, and N 1s were significantly enhanced. The C 1s high-resolution spectrum of CDs was resolved into three peaks corresponding to surface adsorbed carbon (~285 eV), -COOH (~288 eV), and CO_3^{2-} (~291 eV) groups[22b, 24c, 26]. The C 1s high-resolution spectrum of ZLAGC only had an adsorbed carbon peak, while the C 1s high-resolution spectra of ZLAGC@CDs and CDs were similar in shape. After ZLAGC encapsulation of CDs, the -COOH functional group increased. The C 1s high-resolution spectra of the three samples were compared, which indicated that CDs were successfully encapsulated onto the surface of ZLAGC. The O 1s high-resolution spectrum of CDs was resolved into two peaks corresponding to surface C-O/C=O (~532 eV) and N=O (~534.5 eV) groups[24b, 24c, 26a]. The O 1s high-resolution spectrum of ZLAGC mainly showed M-O bonds (~530 eV, M is a metal element), while the O 1s high-resolution spectrum of ZLAGC@CDs had not only M-O bonds but also abundant oxygen-containing groups, indicating successful encapsulation of CDs onto the surface of ZLAGC. These functional groups were beneficial for the solubility and stability of ZLAGC@CDs in aqueous solutions, thereby expanding its practical applications. Figure 4e shows the XPS valence band spectra of the samples. ZLAGC presented photoelectron peaks corresponding to O 2s (~23 eV), Ga 3d (~19 eV), Zn 3d (~10 eV), and O 2p (~5 eV) orbitals in the low binding energy range near the Fermi level. After encapsulation with CDs, the O 2s (~23 eV) orbital photoelectron peak of ZLAGC@CDs was significantly enhanced, and the maximum energy of the valence band top increased from 2.21 eV to 2.87 eV. All the XPS analyses showed that the binding energy increased after CDs coating, which is perhaps due to that the electron transfer between CDs and ZLAGC increased

the binding force after X-ray excitation of the samples[26a, 27]. Figures S6a-c show the SEM morphologies of CD, ZLAGC, and ZLAGC@CDs powders, respectively. CDs formed micrometer-sized agglomerates with a spherical shape, while ZLAGC particles were irregularly shaped at micro- and sub-micrometer scales. The morphology image of ZLAGC@CDs clearly showed that CDs were uniformly encapsulated onto the surface of ZLAGC particles. The elemental analysis results of sample surfaces (Figures S6d-g) indicated that Al, Zn, Ga, O, and C elements were uniformly distributed in the samples, further confirming that CDs were uniformly encapsulated onto the surface of ZLAGC particles.

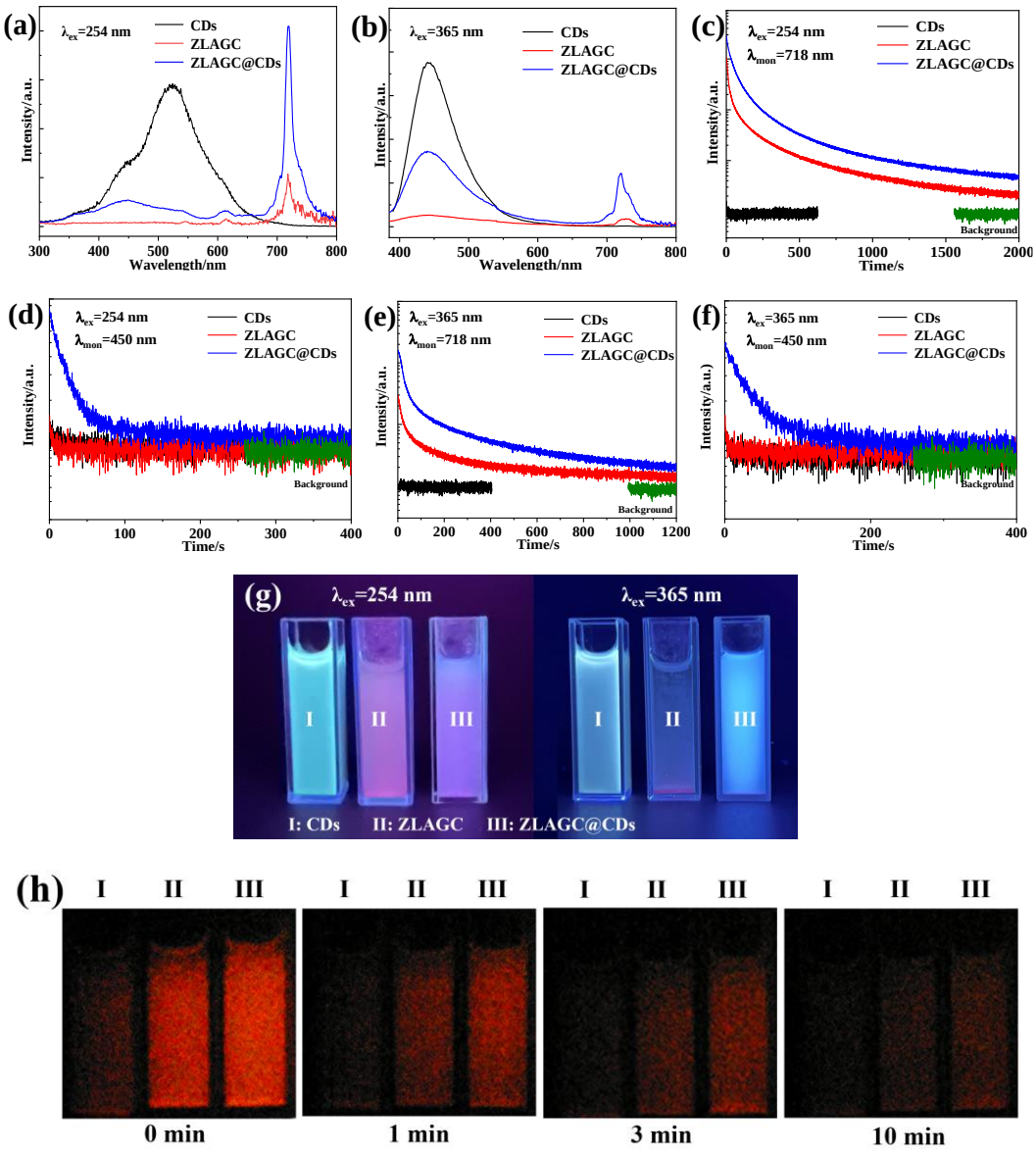

Figure 5. (a, b) PL spectra, (c-f) persistent luminescence curves, (g) digital

photographs, and (h) NIR afterglow images of CDs, ZLAGC, and ZLAGC@CDs taken after UV light excitation.

The photoluminescence properties of aqueous solutions (0.1g/mL) of CDs, ZLAGC, and ZLAGC@CDs composite phosphors were analyzed, as depicted in Figure 5. The PL spectra obtained under different UV excitations showed distinct differences (Figure 5a and 5b). Under excitation at wavelengths of 254 nm and 365 nm, broad emission peaks were exhibited in the visible range of 350-650 nm and 400-550 nm, respectively. ZLAGC displayed strong emission at approximately 718 nm ($^2E \rightarrow {}^4A_2$ transition of Cr^{3+}) with 254 nm excitation, but showed weak NIR emission under 365 nm excitation. The PL spectra of ZLAGC@CDs exhibited two emission peaks at around 450 nm and 718 nm, corresponding to the defect emission of CDs and the emission of Cr^{3+}, respectively. The NIR emission intensity was significantly stronger than the visible light emission under 254 nm excitation, while the intensities of visible light and NIR light emission were comparable under 365 nm excitation. The visible and NIR emissions of ZLAGC@CDs composite phosphor were significantly enhanced under UV excitation, resulting in an intensity increase of nearly three times. The enhancement of NIR luminescence after CDs coating indicated the energy transfer processes from CDs to ZLAGC.

Analysis of the fluorescence imaging of CDs, ZLAGC, and ZLAGC@CDs composite phosphor solutions stimulated by UV light at different wavelengths was performed, as shown in Figure 5g. From left to right, the images correspond to aqueous solutions of CDs, ZLAGC, and ZLAGC@CDs. The emitted colors were consistent with the PL spectra. Under 254 nm excitation, CDs emitted blue-green light, ZLAGC emitted pink light, and ZLAGC@CDs emitted violet light. Under 365 nm excitation, CDs emitted blue-green light, ZLAGC emitted very weak light, and ZLAGC@CDs emitted blue light. The emission behavior of ZLAGC@CDs exhibited clear dependence on the excitation wavelength.

The persistence luminescence analysis of CDs, ZLAGC, and ZLAGC@CDs composite phosphor solutions was conducted, and the decay curves under different UV excitations were shown in Figure 5c-5f. After exposure to UV excitation, no

afterglow signal was observed for visible light or NIR light monitoring, indicating the absence of persistent luminescence in CDs. The ZLAGC samples exhibited NIR afterglow with a duration of over 2000 s, and the afterglow intensity was stronger after 254 nm excitation than that after 365 nm excitation. The visible light afterglow signal was not detected for ZLAGC samples under different UV excitation. After the CDs coating, the visible and NIR afterglow signals of ZLAGC@CDs composite phosphors were significantly enhanced, which can be inferred from the decay curves. This enhancement can be attributed to the defects in CDs enhancing the light storage capacity of ZLAGC, reflecting the energy transfer of CDs emission to the splitting trap, which leads to the enhancement of afterglow. The NIR afterglow images of the composite phosphor solution of CDs, ZLAGC, and ZLAGC@CDs after 254 nm excitation for 5 min were shown in Figure 5h. CDs exhibited almost no NIR afterglow, while the coating of ZLAGC phosphor by CDs increased the afterglow intensity of ZLAGC@CDs, which corresponded to the decay curve. This further demonstrated that the CDs coating on ZLAGC improved the afterglow behavior of the samples. Compared with ZLAGC@CDs, there was a small improvement in the NIR afterglow performance of ZGC by coated CDs (Figure S10 and S11), which indicates that the split deep trap promoted the tunneling effect between deep trap and CDs defect level. To understand this enhancement effect in more detail, the fluorescence lifetime was investigated. As shown in Figure S12, CDs and ZLAGC@CDs were excited at an excitation wavelength of λ_{ex}=249 nm, and the decay time have been measured and the lifetimes have been calculated with a biexponential fit. The fast decay directly after excitation in curves can be attributed to the Raman scattering of water. It is clearly visible that the decay of ZLAGC@CDs (1.76 ns) is much faster than CDs (3.75 ns), which can prove the energy transfer processes from CDs to ZLAGC[28].

Based on the above analysis, a schematic diagram summarizing the preparation of ZLAGC@CDs samples as well as the excitation, emission, and afterglow processes of composite phosphor was presented in Figure 6. The successful combination of blue-green emitting CDs with ZLAGC yielded a composite phosphor with double emissions of blue and NIR. Normally, under UV excitation, electrons of ZLAGC were

excited from the valence band to the conduction band, resulting in excited electrons and holes. The electrons of Cr^{3+} ions were promoted from the ground state $^4A_2$ to excited states, followed by relaxation to the ^2E level and subsequent transition back to the $^4A_2$ ground state, resulting in NIR luminescence at ~718 nm. Meanwhile, ground state electrons in Cr^{3+} and the valence band were excited to the conduction band. Subsequently, the electrons were captured by the traps located near the conduction band. Upon the cessation of UV excitation, the trapped electrons were released and recombined with the excited state levels of Cr^{3+}, resulting in NIR afterglow emission[1a, 3a, 3c]. Upon excitation of CDs, electrons transitioned from HOMO to LUMO, relaxed to the defect state, and radiatively transitioned back to HOMO, resulting in blue fluorescence[10, 13, 26a].

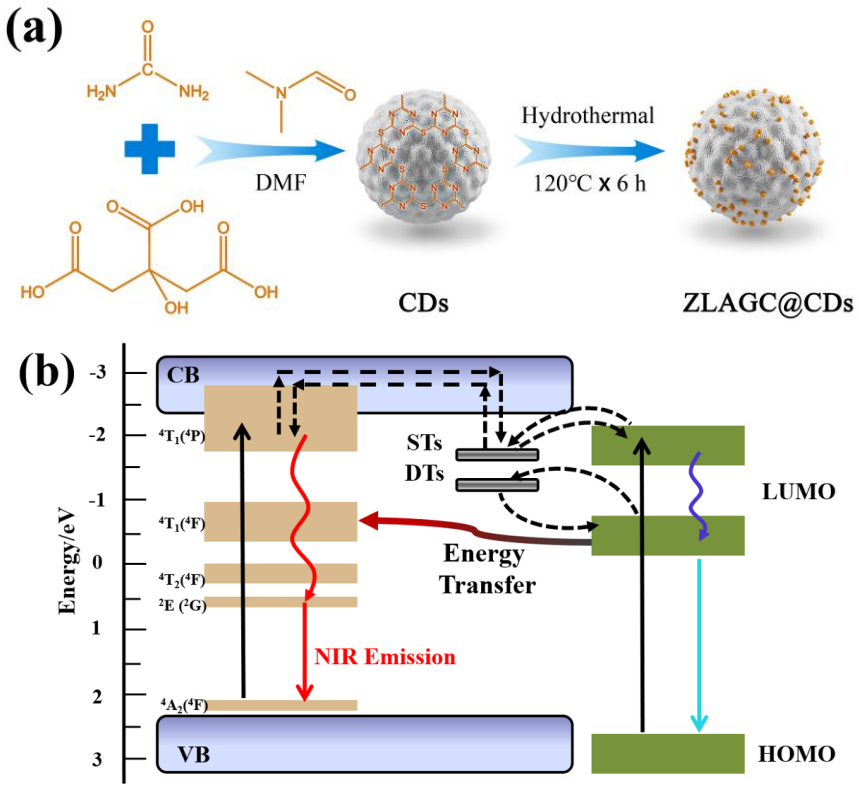

Figure 6. (a) Schematic illustration for the preparation of ZLAGC@CDs samples. (b) Schematic diagram of the proposed luminescence mechanism of ZLAGC@CDs

In the schematic diagram of ZLAGC@CDs, there are three characteristic energy transfer processes: (1) The enhanced NIR emission of Cr^{3+}. The electrons on LUMO were transferred to the excited states of neighboring Cr^{3+} ions, followed by non-radiative relaxation to the 2E state, and finally transitioned to the $^4A_2$ ground state,

leading to the enhanced NIR emission of Cr^{3+}. (2) The enhanced NIR afterglow. The splitting of trap levels in ZLAGC facilitated the transfer of electrons between the deep traps and LUMO. After UV excitation, the traps not only capture the electrons on the conduction band, but also the electrons on the LUMO of the CDs transfer to the deep trap through the heterojunction, which leads to the enhancement of the NIR afterglow. (3) The enhanced visible light afterglow. Obviously, achieving effective radiation transition under UV irradiation to visible light afterglow is difficult. Fortunately, the LUMO energy levels of CDs are just matched with the split deep trap energy levels of ZLAGC, which transfer the electrons from deep traps to the LUMO of CDs and enhanced visible light afterglow.

3.3 Acid fluorescence detection of ZLAGC@CDs

It has been reported that changes in pH can alter the molecular or electronic structure of certain CDs, resulting in changes in the emission wavelength and fluorescence intensity, thereby making them pH-dependent[24a, 29]. In this study, the photoluminescence analysis of the ZLAGC@CDs composite phosphor aqueous solution (0.1g/mL) was performed under different pH conditions. Figures 7a and 7b show the PL spectra obtained under different UV light excitations, respectively. It can be observed that under acidic conditions, the fluorescence intensity gradually decreased with decreasing pH value. At pH=7, the fluorescence intensity of ZLAGC@CDs was approximately 3-4 times higher than that at pH=1. Under acidic pH conditions, the protonation of amino/amide groups resulted in the destruction of the C-N/C=N fluorescence source, leading to a decrease in the π-π* and n-π* transitions and ultimately resulting in fluorescence quenching[6a, 24a]. Figure 7g displays the digital photos of the ZLAGC@CDs composite phosphor aqueous solution excited by UV light at different wavelengths under different pH conditions. Successively shown from left to right are the aqueous solutions of the ZLAGC@CDs composite phosphor solution at pH=1, pH=3, pH=5, and pH=7. As the pH decreased, the observed purple-red luminescence intensity of ZLAGC@CDs gradually increased under 254 nm excitation. Conversely, the blue luminescence of ZLAGC@CDs gradually decreased under 365 nm excitation, showing a luminous color change

consistent with the PL spectra. Under acidic conditions, ZLAGC@CDs exhibited a promising pH-dependent fluorescence detection ability.

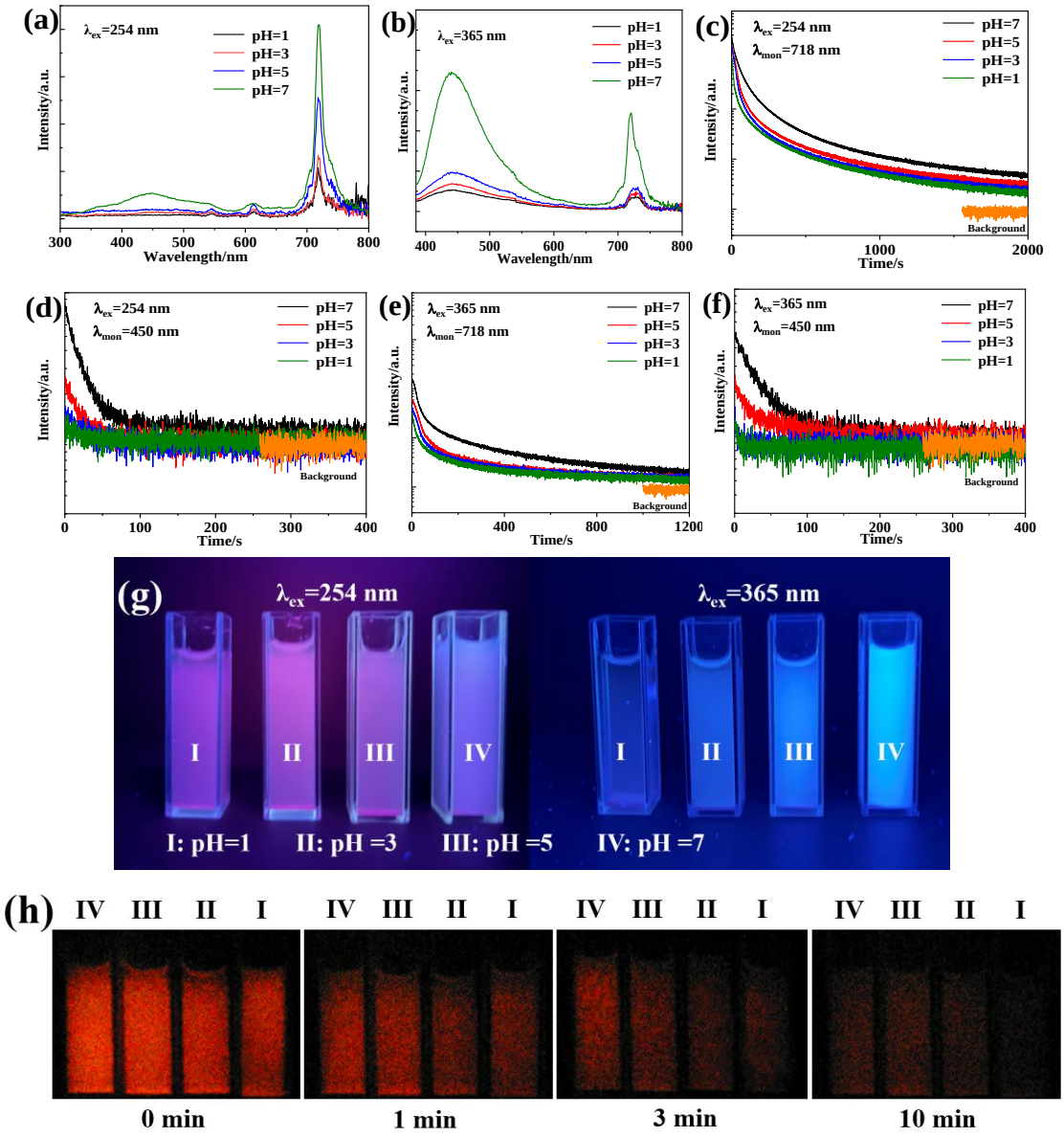

Figure 7. (a, b) PL spectra, (c-f) persistent luminescence curves, (g) digital photographs, and (h) NIR afterglow images of ZLAGC@CDs as a function of the solution pH (1 to 7) under UV excitation.

Persistence analysis of the ZLAGC@CDs composite phosphor aqueous solutions under acidic conditions with different pH values was conducted. The decay curves and persistence imaging are shown in Figure 7c-f and Figure 7h, respectively. Under acidic conditions with decreasing pH values, the residual intensity and duration of both visible and NIR light in ZLAGC@CDs decreased, suggesting weakened energy

transfer from CDs to ZLAGC due to the protonation of functional groups in the sample under acidic pH conditions[23-24].

The pH dependence of the fluorescence intensity of ZLAGC@CDs under alkaline conditions was also investigated. As shown in Figure S13, the digital photos of the samples excited by different UV light showed no significant change in the luminescent color of ZLAGC@CDs with an increase in pH, indicating that changes in pH in alkaline environments did not affect the optical properties of ZLAGC@CDs. Furthermore, the detection of ZLAGC@CDs for other substances was verified. Various ions Na^+, K^+, Mg^{2+}, Zn^{2+}, Ca^{2+}, Cd^{2+}, Li^+ and H^+, 0.1 M) and bioactive molecules (Glucose, GSH, Cys, Asp, Gln, etc.) were tested at a concentration of 5 mM. The fluorescence intensities at the two emission wavelengths are shown in Figure S14. Compared to the fluorescence intensity of ZLAGC@CDs in the aqueous solution at pH 7, there were no significant changes in the fluorescence intensity of the solutions containing other substances, except for a sharp drop in the fluorescence intensity of the solution containing H^+ (0.1 M, pH=1). This indicates that ZLAGC@CDs exhibited no significant signal response to these substances and that these substances did not interfere with the fluorescence signals. These results demonstrate that ZLAGC@CDs showed high sensitivity to H^+ and was unaffected by other ions and bioactive molecules.

4. Conclusion

In this study, a series of $Zn_{1-x}(Li/Al)_xGa_{2x}O_4:0.005Cr^{3+}$ (x=0-1) NIR persistent luminescent phosphors were synthesized by solid-state reaction. Then ZLAGC@CDs composite luminescent material was prepared by hydrothermal reaction. The samples were Characterized by XRD, PLE/PL, TL, FT-IR, XPS spectra and persistent luminescence decay analysis. The substitution of Zn^{2+} by Li^+/Al^{3+} ions leads to the splitting of the trap energy level, thus promoting the tunneling effect between deep trap and CDs defect level. After coating, energy transfer between defect level of CDs to excited state of Cr^{3+} ions takes place, which contributes to a unique double enhanced emission at ~430 and 718 nm. The electron transfer between the defect level

of CDs and the split deeper trap level of ZLAGC also improves the visible and NIR afterglow. The fluorescence and afterglow signals of ZLAGC@CDs are highly sensitive to solution pH under acidic conditions, which provides new applications of acid microenvironment fluorescence detection.

Conflicts of interest

The authors declare that they have no conflict of interest.

Supporting Information

Supporting Information is available from the Wiley Online Library.

Acknowledgements

This work was supported in part by the Fundamental Research Funds for the Central Universities (Grant N2302004) and National Natural Science Foundation of China (Grant 52371057, U21A2045, 52172112).

References

[1] a) Z. Pan, Y. Y. Lu, F. Liu, *Nat. Mater.* **2011**, 11, 58; b) T. Maldiney, A. Bessiere, J. Seguin, E. Teston, S. K. Sharma, B. Viana, A. J. Bos, P. Dorenbos, M. Bessodes, D. Gourier, D. Scherman, C. Richard, *Nat. Mater.* **2014**, 13, 418; c) A. Abdukayum, J. T. Chen, Q. Zhao, X. P. Yan, *J. Am. Chem. Soc.* **2013**, 135, 14125.

[2] a) Z. Li, Y. Zhang, X. Wu, L. Huang, D. Li, W. Fan, G. Han, *J. Am. Chem. Soc.* **2015**, 137, 5304; b) R. Zou, J. Huang, J. Shi, L. Huang, X. Zhang, K.-L. Wong, H. Zhang, D. Jin, J. Wang, Q. Su, *Nano Res.* **2017**, 10, 2070; c) J. Shi, X. Sun, J. Li, H. Man, J. Shen, Y. Yu, H. Zhang, *Biomaterials* **2015**, 37, 260; d) J. Xiahou, Q. Zhu, F. Li, M. Jin, L. Zhu, S. Huang, T. Zhang, X. Sun, J.-G. Li, *Inorg. Chem. Front.* **2023**, 10, 2174.

[3] a) A. Bessière, S. K. Sharma, N. Basavaraju, K. R. Priolkar, L. Binet, B. Viana, A. J. J. Bos, T. Maldiney, C. Richard, D. Scherman, D. Gourier, *Chem. Mater.* **2014**, 26, 1365; b) M. Allix, S. Chenu, E. Véron, T. Poumeyrol, E. A. Kouadri-Boudjelthia, S. Alahraché, F. Porcher, D. Massiot, F. Fayon, *Chem. Mater.* **2013**, 25, 1600; c) Y. Zhuang, J. Ueda, S. Tanabe, *J. Mater. Chem. C* **2013**, 1, 7849.

[4] a) A. Fernández-Osorio, M. Tapia, A. R. Vázquez-Olmos, J. Chávez, *J. Solid State Chem.* **2019**, 269, 328; b) Y. X. Zhuang, J. Ueda, S. Tanabe, P. Dorenbos, *J. Mater. Chem. C* **2014**, 2, 5502.

[5] a) J. Q. Xiahou, Q. Zhu, L. Zhu, S. Huang, T. Zhang, X. D. Sun, J.-G. Li, *J. Mater. Chem. C* **2022**, 10, 7935; b) Y. Chen, J. Chen, J. Liang, J. He, Z.-Q. Liu, Y. Yin, *Chem. Mater.* **2020**, 32, 9551; c) X.-B. Li, W.-T. Huang, R.-R. Zhang, Y. Guo, H.-J. Yang, X.-Y. He, M.-X. Yu, L.-X. Wang, Q.-T. Zhang, *Rare Metals* **2021**, 41, 1230.

[6] a) V. Georgakilas, J. A. Perman, J. Tucek, R. Zboril, *Chem. Rev.* **2015**, 115, 4744; b) S. J. Zhu, Y. B. Song, X. H. Zhao, J. R. Shao, J. H. Zhang, B. Yang, *Nano Res.* **2015**, 8, 355.

[7] a) X. M. Li, M. C. Rui, J. Z. Song, Z. H. Shen, H. B. Zeng, *Adv. Funct. Mater.* **2015**, 25, 4929; b) S. Y. Lim, W. Shen, Z. Gao, *Chem. Soc. Rev.* **2015**, 44, 362.

[8] a) W. Shao, G. Chen, A. Kuzmin, H. L. Kutscher, A. Pliss, T. Y. Ohulchanskyy, P. N. Prasad, *J. Am. Chem. Soc.* **2016**, 138, 16192; b) W. Zou, C. Visser, J. A. Maduro, M. S. Pshenichnikov, J. C. Hummelen, *Nat. Photonics* **2012**, 6, 560; c) G. Chen, J. Damasco, H. Qiu, W. Shao, T. Y. Ohulchanskyy, R. R. Valiev, X. Wu, G. Han, Y. Wang, C. Yang, H. Agren, P. N. Prasad, *Nano Lett.* **2015**, 15, 7400.

[9] a) B. Wang, Y. Yu, H. Zhang, Y. Xuan, G. Chen, W. Ma, J. Li, J. Yu, *Angew. Chem. Int. Ed. Engl.* **2019**, 58, 18443; b) B. Wang, Y. Mu, H. Zhang, H. Shi, G. Chen, Y. Yu, Z. Yang, J. Li, J. Yu, *ACS Cent Sci* **2019**, 5, 349.

[10] Z. Li, Y. Zhao, K. Huang, L. Huang, Y. Zhang, H. Yang, G. Han, *Angew. Chem. Int. Ed. Engl.* **2021**, 60, 15886.

[11] W. Shi, J. Yao, L. Bai, C. Lu, *Adv. Funct. Mater.* **2018**, 28.

[12] J. He, Y. Chen, Y. He, X. Xu, B. Lei, H. Zhang, J. Zhuang, C. Hu, Y. Liu, *Small* **2020**, 16, e2005228.

[13] Z. Song, Y. Liu, X. Lin, Z. Zhou, X. Zhang, J. Zhuang, B. Lei, C. Hu, *ACS Appl. Mater. Interfaces* **2021**, 13, 34705−34713.

[14] J. Q. Xiahou, Q. Zhu, L. Zhu, S. Y. Li, J.-G. Li, *ACS Appl. Electron. Mater.* **2021**, 3, 3789.

[15] a) Y. Q. Sun, X. J. Zhang, J. L. Zhuang, H. R. Zhang, C. F. Hu, M. T. Zheng, B. F. Lei, Y. L. Liu, *Carbon* **2020**, 165, 306; b) C. X. Peng, X. Chen, M. L. Chen, S. C. Lu, Y. Wang, S. L. Wu, X. W. Liu, W. Huang, *Research* **2021**, 2021, 1.

[16] Z. Gong, Y. Liu, J. Yang, D. Yan, H. Zhu, C. Liu, C. Xu, H. Zhang, *Phys. Chem. Chem. Phys.* **2017**, 19, 24513.

[17] a) M. Back, E. Trave, J. Ueda, S. Tanabe, *Chem. Mater.* **2016**, 28, 8347; b) T. Si, Q. Zhu, J. Q. Xiahou, X. D. Sun, J.-G. Li, *ACS Appl. Electron. Mater.* **2021**, 3, 2005; c) Y. Li, Y. Y. Li, R. C. Chen, K. Sharafudeen, S. F. Zhou, M. Gecevicius, H. H. Wang, G. P. Dong, Y. L. Wu, X. X. Qin, J. R. Qiu, *NPG Asia Materials* **2015**, 7, e180; d) Q. Y. Bai, S. L. Zhao, L. Guan, Z. J. Wang, P. L. Li, Z. Xu, *Cryst. Growth Des.* **2018**, 18, 3178.

[18] a) R. Chen, *J. Electrochem. Soc.* **1969**, 116, 1254; b) R. Chen, *J. Appl. Phys.* **1969**, 40, 570.

[19] I. Villa, A. Lauria, F. Moretti, M. Fasoli, C. Dujardin, M. Niederberger, A. Vedda, *Phys. Chem. Chem. Phys.* **2018**, 20, 15907.

[20] a) X. D. Wang, O. S. Wolfbeis, R. J. Meier, *Chem. Soc. Rev.* **2013**, 42, 7834; b) H. Zhu, C. C. Lin, W. Luo, S. Shu, Z. Liu, Y. Liu, J. Kong, E. Ma, Y. Cao, R. S. Liu, X. Chen, *Nat. Commun.* **2014**, 5, 4312.

[21] a) M. Li, H. Zhang, X. Zhang, J. Deng, Y. Liu, Z. Xia, B. Lei, *Mater. Res. Bull.* **2018**, 108, 226; b) J. Ueda, M. Back, M. G. Brik, Y. Zhuang, M. Grinberg, S. Tanabe, *Opt. Mater.* **2018**, 85, 510.

[22] a) C. L. Xia, S. J. Zhu, T. L. Feng, M. X. Yang, B. Yang, *Adv. Sci.* **2019**, 6, 1901316; b) D. Qu, M. Zheng, J. Li, Z. G. Xie, Z. C. Sun, *Light Sci. Appl.*

2015, 4, e364; c) M. Cao, Y. Liu, M. Zhu, J. Xia, T. Xuan, D. Jiang, G. Zhou, H. Li, *J. Alloys Compd.* **2021**, 873.

[23] Y. F. Wang, A. G. Hu, *J. Mater. Chem. C* **2014**, 2, 6921.

[24] a) U. Baruah, M. J. Deka, D. Chowdhury, *RSC Adv.* **2014**, 4, 36917; b) H. Ding, J. S. Wei, P. Zhang, Z. Y. Zhou, Q. Y. Gao, H. M. Xiong, *Small* **2018**, 14, 1800612; c) K. Jiang, Y. Wang, C. Cai, H. Lin, *Adv. Mater.* **2018**, 30, 1800783; d) W. Lu, X. Qin, S. Liu, G. Chang, Y. Zhang, Y. Luo, A. M. Asiri, A. O. Al-Youbi, X. Sun, *Anal. Chem.* **2012**, 84, 5351.

[25] a) Q. Zhu, J. Q. Xiahou, Y. Guo, H. L. Li, C. Ding, J. Wang, X. D. Li, X. D. Sun, J.-G. Li, *ACS Appl. Bio Mater.* **2018**, 2, 577; b) H. Stöffler, T. Zinkevich, M. Yavuz, A. Senyshyn, J. Kulisch, P. Hartmann, T. Adermann, S. Randau, F. H. Richter, J. Janek, S. Indris, H. Ehrenberg, *The Journal of Physical Chemistry C* **2018**, 122, 15954; c) O. Q. De Clercq, L. I. D. J. Martin, K. Korthout, J. Kusakovskij, H. Vrielinck, D. Poelman, *J. Mater. Chem. C* **2017**, 5, 10861.

[26] a) H. Ding, S. B. Yu, J. S. Wei, H. M. Xiong, *ACS Nano* **2016**, 10, 484; b) T. Zhang, J. Zhu, Y. Zhai, H. Wang, X. Bai, B. Dong, H. Wang, H. Song, *Nanoscale* **2017**, 9, 13042.

[27] a) Y. O. Zagorodniy, V. Chlan, H. Štěpánková, Y. Fomichov, J. Pejchal, V. V. Laguta, M. Nikl, *J. Phys. Chem. Solids* **2019**, 126, 93; b) Q. Zhu, J. Q. Xiahou, X. D. Li, X. D. Sun, J. G. Li, *J. Am. Ceram. Soc.* **2021**, 104, 4594.

[28] a) W. Becker, *J. Microsc.* **2012**, 247, 119; b) J. Páterek, M. Pokorný, S. Sýkorová, A. Stehlík, J. Polák, J. Houžvička, M. Nikl, *J. Lumin.* **2019**, 213, 469; c) X. Bian, Q. Shi, C. e. Cui, L. Wang, Y. Tian, B. Xu, Z. K. Mamytbekov, P. Huang, *Mater. Res. Bull.* **2019**, 110, 102; d) A. Ito, T. J. Meyer, *Phys. Chem. Chem. Phys.* **2012**, 14, 13731.

[29] a) R. Das, R. Bandyopadhyay, P. Pramanik, *Materials Today Chemistry* **2018**, 8, 96; b) H. Ehtesabi, Z. Hallaji, S. Najafi Nobar, Z. Bagheri, *Mikrochim. Acta* **2020**, 187, 150; c) Y. Dong, R. Wang, G. Li, C. Chen, Y. Chi, G. Chen, *Anal. Chem.* **2012**, 84, 6220.

Junqing Xiahou is currently a PhD student at the School of Materials Science and Engineering, Northeastern University, China. His research interest focuses on the near-infrared (NIR) persistent luminescent phosphors.

Qi Zhu received his doctor's degree of engineering in materials science from Northeastern University, China in 2012. He is now a full professor of materials science and engineering at Northeastern University, China. He was a guest researcher at National Institute for Materials Science (NIMS, Japan) in 2009-2011, and as a visiting researcher at NIMS in 2018-2019. His research interests include the design, syntheses, and application of optically functional inorganic materials. To date, he has published over 100 scientific papers on optically functional inorganic materials.

Ji-Guang Li received his doctor's degree of engineering in materials science from Northeastern University, China in 1998. He joined the National Institute for Materials Science, Japan in 2001, after completing two years of research at the National Institute for Research in Inorganic Materials, Japan as an STA (science and technology agency) Fellow, and is now a Chief Researcher. He has authored more than 230 peer reviewed research papers and is a holder of 27 patents. His research papers were cited more than 5000 times and showed a citation h-index of 52 (google scholar). His research interests include powder technology and optically functional inorganic materials, mainly including transparent ceramics, photocatalysts and phosphors.

The ZLAGC@CDs phosphors exhibit double emissions at ~430 and 718 nm. The CDs→Cr^{3+} energy transfer enhances the NIR emission. The interaction between CDs and electron traps improves visible/NIR afterglow. The phosphors are fluorescence sensor for acid microenvironment detection.

Junqing Xiahou, Li Cao, Sai Huang, Tao Zhang, Ji-Guang Li*, and Qi Zhu*

Grafting carbon dots on persistent luminescence phosphors to generate remarkably improved NIR afterglow for microenvironment fluorescence detection

ToC figure